 itation information: DOI 10.1109/TPEL.2017.2677527, IEEE

Stator Harmonic Currents Suppression for DFIG Based on Feed-forward Regulator Under Distorted Grid Voltage

Chao Wu, Heng Nian, Senior *Member, IEEE*

***Abstract*—This paper presents a stator harmonic currents suppression method for DFIG under distorted grid voltage. In the proposed control strategy, the feed-forward regulator instead of the resonant regulator is employed to eliminate the negative impacts on the stator current caused by the distorted grid voltage. The leading phase compensator is applied to compensate the system delay when the sampling frequency is low. This approach can provide both the good dynamic response and strong rejection ability against the stator harmonic voltages. Based on the stator current model of DFIG, the feed-forward regulator is designed in detail. The comparison between the resonant controllers and the feed forward regulator is also made on the basis of bode diagram. Then, the robustness against the frequency variations and the parameter deviations are analyzed. Finally, the simulation and experimental results are presented to validate the effectiveness of the proposed control strategy.**

***Index Terms*— Doubly-fed induction generator, stator harmonic currents suppression, feed-forward regulator, distorted grid voltage**

I. INTRODUCTION

Nowadays, the doubly-fed induction generators (DFIGs) have been widely equipped in the wind power generation system due to several advantages, including smaller converters rating around 30% of the generator rating, variable speed and four-quadrant active and reactive power operation capabilities [1]-[3]. However, the wind farms are usually built in the remote area such as offshore or mountainous regions in which the harmonically distorted grid voltage will usually occur. Since the stator of DFIG is directly connected to the grid, the distorted grid voltage will introduce the harmonic components in the stator current which impact generated power quality [4]-[5]. Moreover, the stator harmonic currents will cause the active and reactive power pulsation and electromagnetic torque pulsation. Thus, it is of significant importance to suppress the stator harmonic currents of the DFIG under distorted grid voltage.

In order to suppress the stator harmonic currents of DFIG under distorted grid voltage, several control strategies have been investigated in [6]-[16]. When only considering the 5^{th} and 7^{th} harmonic components of grid voltage, a rotor current controller, consisting of a PI regulator and a harmonic resonant compensator tuned at six times grid voltage frequency, was employed in the positive synchronous reference frame to regulate the stator harmonic currents in [6]-[11]. However, the sequential decompositions of harmonic components in the stator voltage and current are needed to calculate the rotor current reference, which will inevitably introduce control delay. Moreover, the rotor current references are calculated on the basis of accurate DFIG parameters, such as stator inductance, rotor inductance and mutual inductance. If the parameters are not accurate due to the temperature, the skin effects and the flux linkage saturation, the control error is inevitable in the practical situation. In [12], a stator harmonic current control loop was directly added to the conventional rotor current control loop for harmonic suppression, which can avoid the complex reference calculations of rotor harmonic current. However, the stator harmonic current control loop will reduce the bandwidth of the rotor current control loop, which will deteriorate the dynamic response of the rotor current control loop.

In practice, the renewable power generation system has been widely applied in the weak grid, micro grid, or stand-alone power grid. The high order harmonic voltage distortion, including 11^{th}, 13^{th}, 17^{th}, 19^{th}, etc., cannot be ignored in the point of common coupling (PCC) [13]. Then, the control strategies for suppressing the stator harmonic currents under the generalized harmonic grid are investigated in [14]-[18]. In [14]-[15], a repetitive control (RC) regulator was added to the rotor current control loop to mitigate the $6n \pm 1$ harmonic components of stator current. The high pass filter was applied to extract harmonic components of stator current. However, the high pass filter would introduce the magnitude and phase errors of the sampled stator current. Thus, the inaccurate feedback of the stator harmonic currents will occur, which will cause control error of the RC regulator and deteriorate the suppression ability of the harmonic current. In [18], a sort of nonlinear backstepping-based algorithm was presented to suppress the stator harmonic currents for DFIG under the distorted grid voltage. However, the backstepping method is also highly depended on the DFIG parameters.

In a conclusion, the existed control strategies for DFIG under the harmonically distorted grid voltage have several limitations as the following,

1. The stator fundamental current is indirectly regulated by the rotor fundamental current control loop. However, the rotor fundamental current references are calculated on the basis of the commanded powers and the generator parameters [6]-[10]. Thus, the control accuracy of stator current will be inevitably deteriorated due to the DFIG parameters deviation.
2. The stator harmonic current suppression regulator is added into the fundamental current control loop [12], which will

 itation information: DOI 10.1109/TPEL.2017.2677527, IEEE

reduce the bandwidth of the fundamental current control loop and deteriorate the dynamic response of the fundamental current control loop [12].

3. The frequency deviation of the 6n±1 harmonic component is 6n±1 times of the fundamental frequency deviation. Thus, the resonant regulator would fail to suppress the stator harmonic currents if the fundamental frequency deviation is higher due to the limited bandwidth of the resonant regulator [20]-[21].

In this paper, aimed at the generalized grid harmonic voltages, the stator harmonic currents can be suppressed based on the proposed feed-forward regulator, by which the stator harmonic voltages can be directly compensated by the rotor harmonic voltages. The advantages of the proposed method can be concluded as the following,

1. In order to reduce the generator parameter dependency when calculating the current references from the stator power references, the direct stator current vector control is applied in this paper instead of the conventional rotor current vector control [19].

2. The output of feed-forward regulator is directly added to the rotor voltage reference so that the resonant controller can be avoided. Since that the feed forward regulator is not involved in the stator current control loop, thus the bandwidth of the fundamental current control loop is not affected by the stator harmonic currents suppression. Therefore, the dynamic response of the fundamental current is not affected by the feed forward regulator.

3. When the output of feed forward regulator is added into the rotor voltage, the negative influence of the stator harmonic voltages on the stator harmonic currents is counteracted by the feedforward term. The magnitude response of the transfer function from the stator voltage to the stator current can be significantly reduced by the feedforward term. Thus, the feed forward regulator is effective in mitigating the stator harmonic currents even considering the generalized harmonic grid in which the 5-,7+,11-,13+,17-,19+, 6n±1order harmonic voltages are all considered.

4. Since the magnitude responses in the high frequency domain of the transfer function from the stator voltage to the stator current can be reduced by the feedforward term, the proposed control method is robust to the frequency deviation. Even a wide range of frequency deviation is considered, the feed forward regulator is still effective in mitigating the stator harmonic currents, which is advantageous compared to the conventional resonant control scheme.

This paper is organized as follows. The mathematic model of direct stator current control is outlined in Section II. The control strategy of the rotor side controller (RSC) is elaborated in detail in Section III. Furthermore, the design of the feed-forward regulator and the performance analysis of proposed control strategy are presented in Section IV. Section V and VI show the simulation and experimental results respectively. Finally, the conclusions are drawn in Section VII.

II. STATOR CURRENT MODEL

In view of the fact that the vector control of DFIG based on the rotor current is highly depended on the DFIG parameters such as the stator inductance and mutual inductance [19], it is beneficial to employ the direct stator current vector control of the DFIG whose stator winding is directly connected to the grid. In this paper, all the current regulators are designed in the synchronous frame. In order to deduce the mathematic model of stator current vector control, the equivalent circuit of DFIG is built in the synchronous *dq* frame shown as Fig.1, in which *d* axis is oriented in the direction of the fundamental voltage vector.

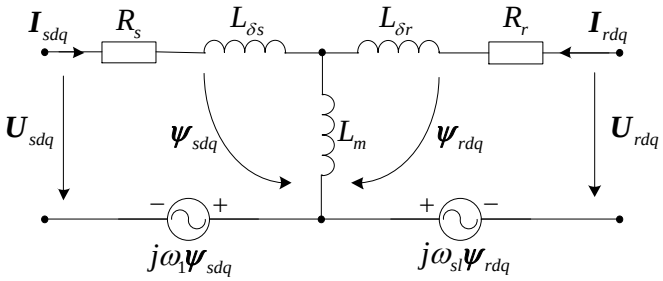

Fig.1 Equivalent circuit of DFIG in the synchronous *dq* frame

According to the equivalent circuit of DFIG in the *dq* frame, the stator/rotor voltages and flux linkages can be expressed as,

$$\begin{cases} \boldsymbol{U}_{sdq} = R_s\boldsymbol{I}_{sdq} + d\boldsymbol{\psi}_{sdq}/dt + j\omega_1\boldsymbol{\psi}_{sdq} \\ \boldsymbol{U}_{rdq} = R_r\boldsymbol{I}_{rdq} + d\boldsymbol{\psi}_{rdq}/dt + j\omega_{sl}\boldsymbol{\psi}_{rdq} \end{cases} \quad (1)$$

$$\begin{cases} \boldsymbol{\psi}_{sdq} = L_s\boldsymbol{I}_{sdq} + L_m\boldsymbol{I}_{rdq} \\ \boldsymbol{\psi}_{rdq} = L_m\boldsymbol{I}_{sdq} + L_r\boldsymbol{I}_{rdq} \end{cases} \quad (2)$$

where R_s and R_r are stator and rotor resistances, ω_{sl} is slip angular frequency, $L_s=L_m+L_{\delta s}$ and $L_r=L_m+L_{\delta r}$ are the self-inductance of stator and rotor windings, $L_{\delta s}$, $L_{\delta r}$ and L_m are the stator and rotor leakage inductances and mutual inductance, respectively.

As can be seen from Fig.1, the inputs of the DFIG are stator voltage and rotor voltage. In order to investigate the control strategy for stator harmonic currents suppression, it is essential to find out the mechanism how the stator and rotor voltage work on the stator current. Thus, the stator current can be designed as the output variable since the control objective is the stator current in this paper.

Then, based on (2), the rotor flux linkage can be expressed in the terms of the stator flux linkage and current as,

$$\boldsymbol{\psi}_{rdq} = L_r\boldsymbol{\psi}_{sdq}/L_m - L_{\delta sr}\boldsymbol{I}_{sdq} \quad (3)$$

where $L_{\delta sr}=L_s\cdot L_r/L_m-L_m$.

Submitting (3) into (1), the rotor voltage can be rewritten as,

$$\boldsymbol{U}_{rdq} = -\left(L_sR_r/L_m\boldsymbol{I}_{sdq} + L_{\delta sr}\,d\boldsymbol{I}_{sdq}/dt + j\omega_{sl}L_{\delta sr}\boldsymbol{I}_{sdq}\right) + \boldsymbol{E}_{rdq} \quad (4)$$

where $\boldsymbol{E}_{rdq}$ is the impact of the stator voltage on the stator current and can be expressed as,

$$\boldsymbol{E}_{rdq} = L_r/L_m\,(R_r/L_r\boldsymbol{\psi}_{sdq} + d\boldsymbol{\psi}_{sdq}/dt + j\omega_{sl}\boldsymbol{\psi}_{sdq}) \quad (5)$$

Ignoring the stator resistance and taking the Laplace transform of (1), (4) and (5), the stator current can be expressed as (6) and the stator current model can be expressed in Fig.2. The stator voltage and rotor voltage are the inputs of the stator current model and the stator current is the output. Thus, the stator current model is built in the synchronous *dq* frame and the input and output are complex variable.

$$\boldsymbol{I}_{sdq} = \frac{L_r\left(R_r/L_r + s + j\omega_{sl}\right)}{\left(s + j\omega_1\right)\left(L_mL_{\sigma rs}s + L_sR_r + j\omega_{sl}L_{\delta sr}L_m\right)}\boldsymbol{U}_{sdq} - \frac{L_m}{L_mL_{\sigma rs}s + L_sR_r + j\omega_{sl}L_{\delta sr}L_m}\boldsymbol{U}_{rdq} \quad (6)$$

itation information: DOI 10.1109/TPEL.2017.2677527, IEEE

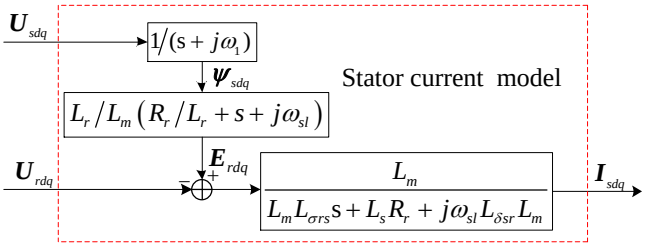

Fig.2 The stator current model of DFIG in the synchronous *dq* frame

As can be seen from (6) and Fig.2, the stator current model can be regarded as a two input and one output system. The output stator current is depended on the input rotor voltage and stator voltage. Thus, the following can be concluded,

1) When the stator voltage is constant, the stator current is only depended on the rotor voltage. In this case, the relationship between the stator current and rotor voltage is simplified as a one order inertial plant, and the required rotor voltage can be directly produced by regulating the stator current through a PI controller. Thus, the stator current can be defined as the controlled variable instead of rotor current, which is the principle of the direct stator current vector control. In this way, the stator current reference calculated from the stator power has no dependency on the generator parameters [19].

2) If the stator voltage is distorted with different order harmonics, the stator flux will also contain harmonics. However, the rotor voltage only contains fundamental voltage if only PI regulator is applied to produce the rotor voltage from the stator current. Thus, the stator harmonic voltages will have a negative impact on the stator current. In this way, the stator current will contain harmonics which are the same orders as the stator voltage harmonics. It is essential to produce appropriate rotor harmonic voltages to eliminate the negative impact of stator harmonic voltages on the stator current.

Based on this two information concluded form the stator current model, the direct stator current vector control is employed to regulate the stator fundamental current and the feed-forward regulator is employed to suppress the stator harmonic currents. The control strategy will be elaborated in detail in section III

III. Stator Current Harmonic Suppression Strategy

For the purpose of suppressing the stator harmonic currents under the generalized grid harmonic voltages, the direct stator current vector control and feed-forward regulator are employed for DFIG control. Fig.3 shows the control block diagram of the proposed stator harmonic currents suppression strategy, in which the PI controller is applied to regulating the stator fundamental current and the feed-forward regulator is added to suppress the stator harmonic currents.

In Fig.3, the sampled distorted grid voltage $\boldsymbol{U}_{sabc}$ is compensated by a leading phase compensator and then transformed to the synchronous *dq* frame as $\boldsymbol{U}_{sdq}$ which is the input of the feed-forward regulator. The second order generalized integrator-based phase-locked loop (SOGI-PLL) block can be used to obtain the orientation angle θ_s and frequency ω_1 of the fundamental positive voltage. The principle of the SOGI-PLL is not repeated in this paper which can be referred in [24]. The rotor speed ω_r and position angle θ_r can be obtained by the encoder output. The stator current $\boldsymbol{I}_{sabc}$ is sampled and transformed to synchronous *dq* frame as $\boldsymbol{I}_{sdq}$ which is used for the stator fundamental current control. The two control loops are described in detail in the following.

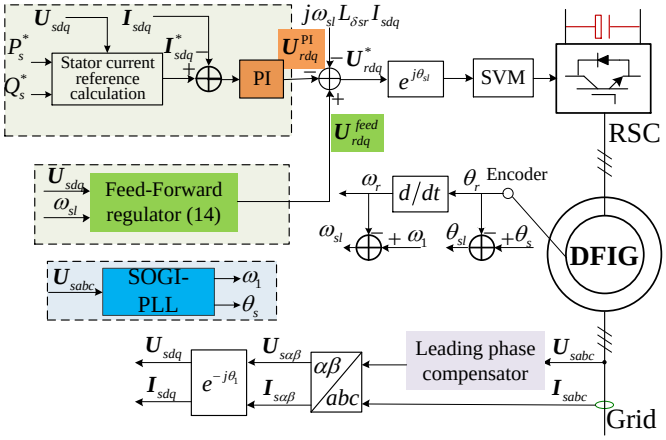

Fig.3 The control scheme of RSC

A. Stator fundamental current control loop

The relationship between the stator power and the stator voltage and stator current in the synchronous *dq* frame can be expressed as,

$$\begin{cases} P_s = U_{sd}I_{sd} + U_{sq}I_{sq} \\ Q_s = U_{sq}I_{sd} - U_{sd}I_{sq} \end{cases} \tag{7}$$

When the stator voltage orientation is achieved by the PLL, the calculation of the stator current reference can be given,

$$\begin{cases} I_{sd}^* = P_s^*/U_{sd} \\ I_{sq}^* = Q_s^*/U_{sd} \end{cases} \tag{8}$$

When the stator voltage is harmonically distorted, the *d*-axis stator voltage also contains the harmonic components. Thus, the *d*-axis stator current reference contains the same order harmonics as the stator voltage. However, only the dc component can be restrained to zero by PI regulator, while the harmonic components can be automatically neglected due to the limited ac signal tracking capability of the PI regulator. Thus, the closed-loop PI control of stator current can have an accurate tracking ability of the stator fundamental current reference and the harmonics existed in the reference caused by the distorted voltage has no negative impact on the stator fundamental current control loop.

Compared with the conventional rotor current vector control strategies, the advantages of the direct stator current vector control can be concluded as the following,

1) The rotor current reference calculation can be avoided. Thus, only stator current sample is necessary and the rotor current transducer can be avoided. However, rotor current transducer is still useful in view of the protection of the RSC. The rotor current dynamics can also be well established in the direct stator current control. When the rotor current exceeds the prescribed limitation during a severe fault, the crowbar is enabled to protect the DFIG system.

2) The calculation of the stator current reference is simpler

 itation information: DOI 10.1109/TPEL.2017.2677527, IEEE

and has no dependency on the generator parameters, which can be seen from (8).

However, the direct stator current vector control can only regulate the fundamental component and has no ability in suppressing the stator harmonic currents. Without applying resonant controllers or repetitive controller in the current control loop, the output of the feed-forward regulator is directly added to the rotor voltage reference to suppress the stator harmonic currents, which will be presented in the next part.

B. Stator harmonic currents control loop

If there is only PI regulator applied in the current control loop, the rotor voltage only contains fundamental component. Thus, the stator harmonic voltages will cause stator harmonic currents which can be seen from the stator current model. In order to eliminate the stator harmonic currents, the rotor harmonic voltages reference should be introduced to counteract the impact of stator harmonic voltages on the stator current.

Then, the key point is how to produce the required rotor harmonic voltages. The resonant controller has been employed to produce the required rotor harmonic voltages in the existing research. However, in this paper, the feed-forward regulator is applied to produce appropriate rotor harmonic voltages to eliminate the negative impact of stator harmonic voltages on the stator current. The output of feed-forward regulator is directly added in the rotor voltage reference. The design of the feed-forward regulator is based on the stator current model shown as Fig.2. The ideal output of the feed-forward regulator can be expressed as,

$$\boldsymbol{U}_{rdq}^{feed}=\boldsymbol{E}_{rdq}=\frac{L_r}{L_m}\frac{R_r/L_r+s+j\omega_{sl}}{s+j\omega_1}\boldsymbol{U}_{sdq} \tag{9}$$

As can be seen from (9), the output of the feed-forward regulator is different from the conventional feed-forward term, which only considers the stator fundamental voltage and current. Since the stator harmonic voltages are considered in (9), it can accurately express the relationship between the stator harmonic voltages and rotor harmonic voltages when stator harmonic currents are suppressed in DFIG.

Since the output of the feed-forward regulator is directly added to the output of PI regulator, the rotor voltage reference can be expressed as,

$$\boldsymbol{U}_{rdq}^{*}=\boldsymbol{U}_{rdq}^{feed}-\boldsymbol{U}_{rdq}^{PI}-j\omega_{sl}L_{\delta sr}\boldsymbol{I}_{sdq} \tag{10}$$

where $\boldsymbol{U}_{rdq}^{feed}$ is the output of the feed-forward regulator, $\boldsymbol{U}_{rdq}^{PI}$ is the output of the PI controller, $j\omega_{sl}L_{\delta sr}I_{sdq}$ is the cross-coupling terms as feed-forward item. The rotor voltage reference is then transformed to the rotor stationary frame, and the space vector modulation is used to obtain the switching signals. The switching signals are then used to drive the RSC and produce the rotor voltage.

IV. Design and Analysis of Feed-Forward Regulator

As can be seen from (9), the expression of the feed-forward regulator is highly depended on the DFIG parameters such as rotor inductance, mutual inductance and rotor resistance which are difficult to acquire the accurate value in the practical operation condition. Hence, the simplification of the feed-forward regulator is necessary. The design of the feed-forward regulator and the performance analysis will be elaborated in this section.

When adding the PI regulator and feed-forward regulator into the stator current control loop, the control block and the stator current model can be shown in Fig.4. In this figure, the transfer function of the feed-forward regulator is expressed as $G_{feed}(s)$, and the transfer function of PI regulator is expressed as $G_{PI}(s)$, $G_1(s)=1/(s+j\omega_1)$, and $G_2(s)=L_r/L_m(R_r/L_r+ s +j\omega_{sl})$, $G_p(s)=L_m/(L_mL_{\sigma rs}s+L_sR_r+ j\omega_{sl}L_mL_{\sigma rs})$.

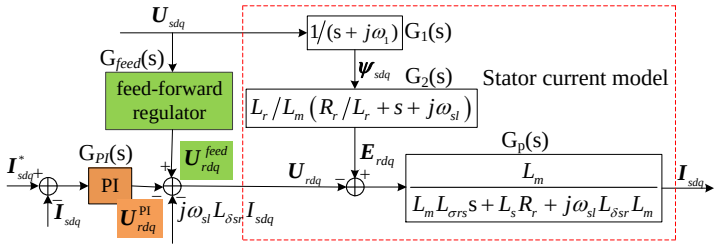

Fig.4 Transfer function diagram of the control strategy

As can be seen from Fig.4, the inputs of the DFIG control system are stator voltage and stator current reference. Thus, the transfer function between the inputs and output can be expressed as,

$$\boldsymbol{I}_{sdq}=\boldsymbol{I}_{sdq}^{*}G_{ii}(s)+\boldsymbol{U}_{sdq}G_{ui}(s) \tag{11}$$

where $G_{ii}(s)$ and $G_{ui}(s)$ can be expressed as,

$$G_{ii}(s)=\frac{G_{\mathrm{PI}}(s)G_{\mathrm{p}}(s)}{1+G_{\mathrm{PI}}(s)G_{\mathrm{p}}(s)} \tag{12}$$

$$G_{ui}(s)=\frac{\left(G_1(s)G_2(s)-G_{feed}(s)\right)G_{\mathrm{p}}(s)}{1+G_{\mathrm{PI}}(s)G_{\mathrm{p}}(s)} \tag{13}$$

The transfer function $G_{ii}(s)$ describes the relationship between the stator current and stator current reference. The transfer function $G_{ui}(s)$ describes the relationship between the stator current and stator voltage. Considering that the practical response of stator current depends on the stator current reference and stator voltage, it is necessary to investigate the bode diagram of the transfer function $G_{ii}(s)$ and $G_{ui}(s)$.

If the feed-forward regulator is not added, the bode diagram of the transfer function $G_{ii}(s)$ and $G_{ui}(s)$ can be plotted as Fig.5. As can be seen from Fig.5, the stator current control loop can achieve a zero steady error for the stator fundamental current and the stator voltage has no effect on the fundamental current. Since the rotor current can be indirectly expressed by the stator flux and stator current, the dynamic performance of the rotor current is the same with the stator current when the stator flux is constant. However, the stator current control loop has no control ability for the harmonic currents and the harmonic voltages will introduce harmonic currents since the $G_{ui}(s)$ is -5dB at 300Hz, -10dB at 600Hz and -14dB at 900Hz, respectively. Thus, if the stator current control loop consisting of PI controller is implemented alone, the stator harmonic currents will be remarkable when the stator voltage is distorted. Thus, the feed-forward regulator is designed to produce appropriate rotor harmonic voltages to compensate the stator harmonic voltages.

 itation information: DOI 10.1109/TPEL.2017.2677527, IEEE

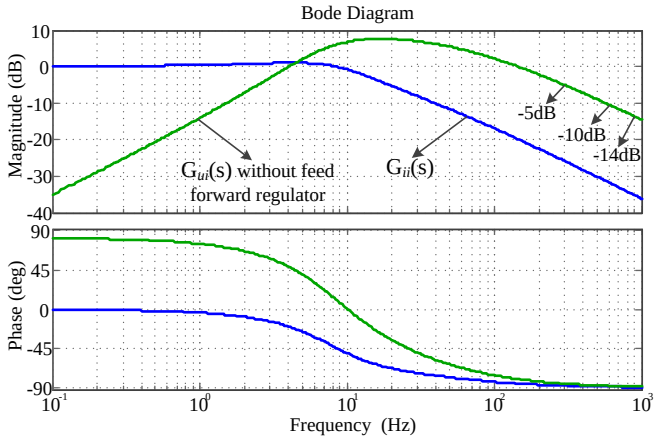

Fig.5 Bode diagram of the transfer function $G_{ii}(s)$ and $G_{ui}(s)$

As can be seen from (12), the feed-forward regulator has no effect on the stator fundamental current control since the feed-forward term is not included in the transfer function $G_{ii}(s)$. Thus, the stator fundamental current control loop can still have good steady and dynamic performance even when the feed-forward regulator is added. Now, the task is to design the $G_{feed}(s)$ to eliminate the impact of the stator voltage on the stator current. Assumed that the transfer function $G_{ui}(s)$ is designed to be zero, the stator voltage would have no impact on the stator current. In this way, no matter how distorted the stator voltage is, the stator current will not contain any harmonic components, which is the control mechanism of the feed-forward regulator.

A. *Design of feed-forward regulator*

As can be seen from (13), if the feed-forward regulator can be expressed as the product of $G_1(s)$ and $G_2(s)$, the stator harmonic currents will be thoroughly eliminated. The ideal feed-forward regulator $G_{feed\_ideal}(s)$ can be expressed as,

$$G_{feed\_ideal}(s)=\frac{L_r}{L_m}\frac{R_r/L_r+s+j\omega_{sl}}{s+j\omega_1} \tag{14}$$

As can be seen in (14), the ideal feed-forward regulator is depended on the DFIG parameters such as rotor inductance, mutual inductance and rotor resistance, which is difficult to be used in the practical situation due to the generator parameters deviation. Thus, the ideal feed-forward regulator should be simplified to meet the robust requirement on the parameters deviation. The design principle of the feed-forward regulator is to make the magnitude and frequency response very close to the ideal feed-forward regulator.

As for the resonant controller or repetitive controller for regulating the harmonic components in the stator currents, the open loop gain of the harmonic frequency point is limited since the bandwidth of these controllers are introduced. In view of this point, there is no need to make the transfer function $G_{ui}(s)$ to be strictly zero. It is also acceptable for $G_{ui}(s)$ to achieve the appropriate attenuation ability to the stator harmonic voltages.

As can be seen from (14), the mutual inductance is almost equal to the rotor inductance and the R_r/L_r term is very small compared with harmonic frequency. Thus, the ideal feed-forward regulator can be simplified as,

$$G_{feed}(s)=\frac{s+j\omega_{sl}}{s+j\omega_1} \tag{15}$$

As can be seen from (15), the feed-forward regulator only has a slip frequency parameter which can be obtained by the position encoder and SOGI-PLL shown as Fig.3.

When the ω_1 is equal to the grid fundamental frequency and the slip is changing from -0.2 to 0.2, the bode diagram of (14) and (15) can be plotted as Fig.6. The dotted lines represent the actual feed-forward regulator $G_{feed}(s)$ and the solid lines represent the ideal feed-forward regulator $G_{feed\_ideal}(s)$.

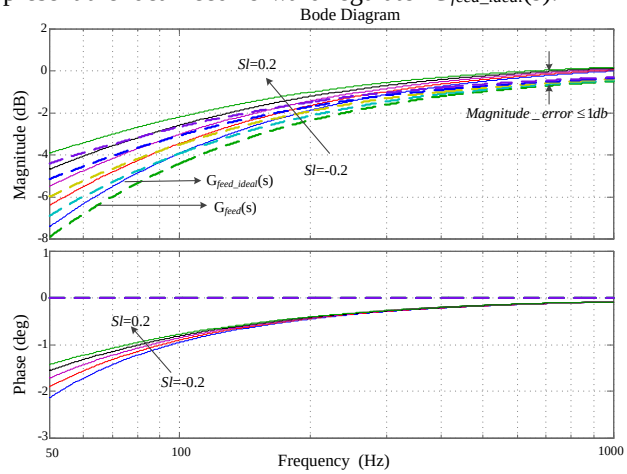

Fig.6 Bode diagram of $G_{feed\_ideal}(s)$ and $G_{feed}(s)$ with different slip

As can be seen from Fig.6, the magnitude error between the ideal and actual feed-forward regulator is less than 1dB. The phase error is less than 2° when the stator frequency is higher than 50Hz in the synchronous *dq* frame. Thus, the ideal feed-forward regulator $G_{feed\_ideal}(s)$ can be substituted by the actual feed-forward regulator expressed as (15), in which no DFIG parameter is contained.

Since (15) has the complex coefficient *j* in the numerator and denominator, its output in the dq reference frame consists of d- and q-axes components. Thus, (15) can be rewritten as,

$$G_{feed}(s)=\frac{s+j\omega_{sl}}{s+j\omega_1}=\frac{s^2+\omega_1\omega_{sl}-j\omega_r s}{s^2+\omega_1^2} \tag{16}$$

As can be seen from (16), the complex coefficient *j* in denominator is eliminated and the complex coefficient *j* in the numerator works as a cross-coupling term. In this way, the block scheme of implementing the feed forward regulator can be shown as,

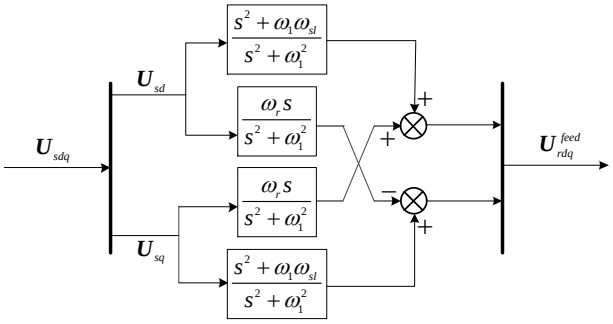

Fig.7 Block scheme of the feed forward regulator

In the block scheme, ω_1 is the grid frequency, ω_r is the rotor speed, ω_{sl} is slip angular frequency. It should be pointed out that ω_r and ω_{sl} are all multiplication coefficients which does not affect the discretization of the feed forward regulator. In the practical application, the bandwidth of the resonant controller is introduced for ensuring the stability of the feed forward regulator.

 itation information: DOI 10.1109/TPEL.2017.2677527, IEEE

When there is no feed-forward regulator added to the rotor voltage reference, the relationship between the stator current and stator voltage can be expressed as,

$$G_{ui}(s)=\frac{G_1(s)G_2(s)G_p(s)}{1+G_{PI}(s)G_p(s)} \tag{17}$$

When the feed-forward regulator expressed as (15) is added to the rotor voltage reference, the relationship between the stator current and stator voltage can be expressed as,

$$G_{ui\_feed}(s)=\frac{\left(G_1(s)G_2(s)-\frac{s+j\omega_{sl}}{s+j\omega_1}\right)G_p(s)}{1+G_{PI}(s)G_p(s)} \tag{18}$$

Combining (16) and (17), the bode diagram of the $G_{ui}(s)$ without feed-forward regulator and the $G_{ui\_feed}(s)$ with feed-forward regulator can be plotted in Fig.8.

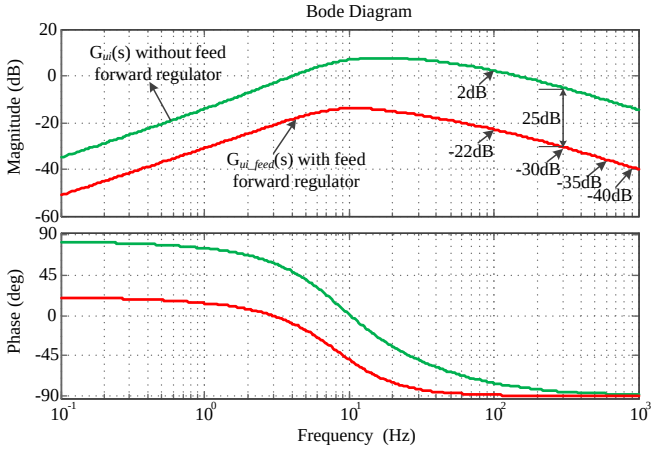

Fig.8 Bode diagram of $G_{ui}(s)$ with and without feed-forward regulator

As can be seen from Fig.8, the response of the stator voltage on the stator current has a good attenuation ability when the feed-forward regulator is added to the rotor voltage reference. The magnitude response is -30dB at 300Hz, -35dB at 600Hz and -40dB at 900Hz, respectively. The magnitude response of $G_{ui}(s)$ is -5dB at 300Hz, -10dB at 600Hz and -15dB at 900Hz without feed-forward regulator. When the feed-forward regulator is not added in the control loop, the harmonic component of stator current at 300Hz will be high, which will deteriorate the output power quality of DFIG system. Since the attenuation magnitude is 25 dB at 300Hz with the feed-forward regulator, the stator current component at 300Hz can be controlled less than one percent of the rated current. As for the higher order harmonics, the attenuation magnitude is larger which indicates a stronger stator harmonic currents suppression ability. Thus, the actual feed-forward regulator proposed as (15) is effective in suppressing the stator harmonic currents which are caused by the stator harmonic voltages. As for the unbalanced grid voltage condition, the negative voltage component is 100Hz in the positive synchronous dq frame. As can be seen from Fig.8, the magnitude response of $G_{ui}(s)$ reduces from 2dB to -22dB when adding the feed forward regulator. Thus, the feed forward regulator is still effective in mitigating the unbalanced stator current caused by the unbalanced grid voltage.

B. Performance comparison of resonant controller and feed forward regulator

In order to compare the performance of the resonant controllers with feed forward regulator, the transfer functions and the bode diagrams are used to compare the dynamic and steady performance of these two control methods.

When applying the resonant controllers and considering the high order harmonics, a series of resonant controllers should be applied just as the following expression.

$$G_R(s)=\frac{2k_r\omega_c s}{s^2+2\omega_c s+(6\omega_1)^2}+\frac{2k_r\omega_c s}{s^2+2\omega_c s+(12\omega_1)^2}+\frac{2k_r\omega_c s}{s^2+2\omega_c s+(18\omega_1)^2} \tag{19}$$

where k_r is the gain and ω_c is the bandwidth of the resonant controller. The bandwidth is applied to take account of the inaccuracy of the stator frequency, whose range is always designed from 5 to 20 rad/s. In the later comparison with feed forward regulator, k_r is 1000 and ω_c is 10 rad/s.

When the resonant controllers are added in the stator current control loop, the transfer function from the stator voltage to the stator current can be express as,

$$G_{ui}(s)=\frac{G_1(s)G_2(s)G_p(s)}{1+\left(G_{PI}(s)+G_R(s)\right)G_p(s)} \tag{20}$$

The bode diagram of the transfer function from the stator voltage to the stator current when applying the resonant controllers can be shown as the Fig.8.

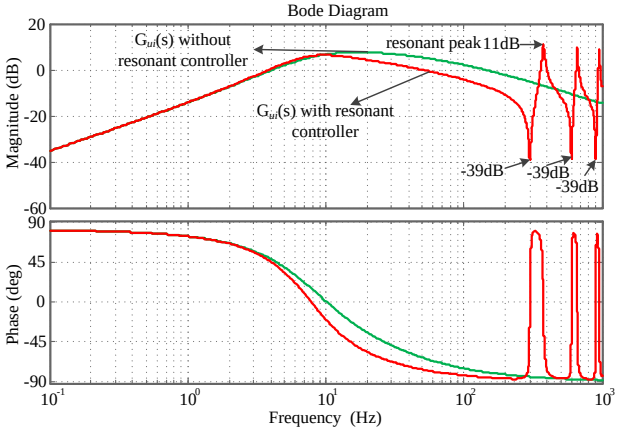

Fig.9 Bode diagram of $G_{ui}(s)$ with and without resonant controller

As can be seen from Fig.8, a good attenuation can also be achieved at the specified frequency such as 300Hz, 600Hz, 900Hz. However, not all magnitude response is attenuated in the high frequency domain. It can be seen that a resonance peak will occur at some frequency point in the frequency domain which is caused by the resonant controller. This will potentially deteriorate the stator current response when the sudden stator voltage dips occur.

When the feed forward regulator is applied in the RSC control scheme, the transfer function from the stator voltage to the stator current can be expressed as (17). As can be seen from Fig.7, a good attenuation of $G_{ui}(s)$ with the feed forward regulator can be achieved in the high frequency domain not only in the given frequency point. Furthermore, there is not any resonance peak in the magnitude response which indicates that the control method has a good anti-disturbance ability against grid voltage.

When considering the dynamic performance comparison of

itation information: DOI 10.1109/TPEL.2017.2677527, IEEE

the resonant controller and feed forward regulator, the transfer functions from the stator current reference to the stator current of these two methods are developed respectively.

When the resonant controller is applied, the transfer function from the rotor current reference to the stator current can be expressed as,

$$G_{ii}(s)=\frac{G_{\mathrm{PI}}(s)G_{\mathrm{p}}(s)}{1+G_{\mathrm{PI}}(s)G_{\mathrm{p}}(s)+G_{\mathrm{R}}(s)G_{\mathrm{p}}(s)} \tag{21}$$

When the feed forward regulator is applied, the transfer function from the stator current reference to the stator current can be expressed as (12),

The bode diagram of these two functions can be plotted as the following figure,

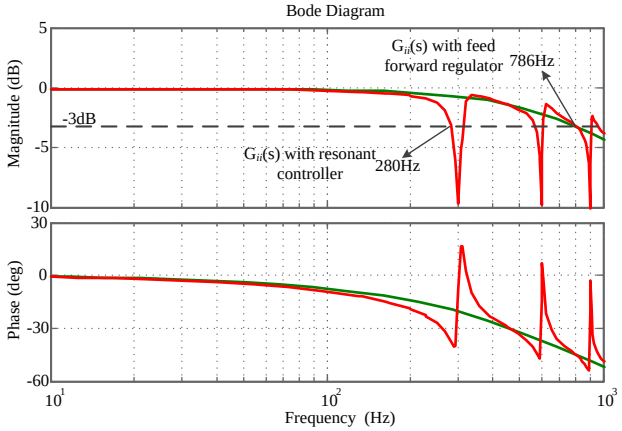

Fig.10 Bode diagram of $G_{ii}(s)$ with and without resonant controller

As can be seen from this figure, the cutoff frequency of the stator current control loop with the resonant controller is 280Hz and the cutoff frequency is 786Hz with the feed forward regulator. Thus, the dynamic performance of the feed forward regulator is better than resonant regulator.

Thus, compared with the resonant controllers, the feed forward regulator has the following advantages

1. The feed-forward regulator has a quicker current response than the resonant controller. The bandwidth of the stator current control loop is not affected by the feed forward regulator. However, the bandwidth of the stator current control loop is decreased when applying the resonant controller [12].

2. The feed forward regulator is simple and effective in dealing with the frequency deviation since it can make the magnitude response attenuation in the high frequency domain which can be shown as Fig.7. When the frequency is higher than 300Hz, the magnitude response is attenuated to -30dB.

3. The anti-disturbance ability against the grid voltage fault of the feed forward regulator is better than the resonant regulator.

The disadvantage is that the control performance with the feed forward regulator is affected by the sampling accuracy of stator voltage. If the stator voltage is not accurate, the mitigation of stator harmonic current will be decreased accordingly.

C. *Robustness against grid frequency variations*

In order to improve the stator harmonic currents suppression ability of DFIG, the robustness against grid frequency should be taken into consideration. In [8], the bandwidth of RC controller is designed to improve the robustness against grid frequency variations. The frequency variations of the harmonics are larger than the fundamental frequency variation. Thus, the bandwidth of the RC controller is difficult to adjust the high order frequency such as 12th and 18th harmonics in the synchronous frame. However, the bandwidth is not necessary for dealing with the grid frequency variation of the feed-forward regulator proposed in this paper.

When the grid fundamental frequency variations are ±2.0 Hz [14], the 6th, 12th and 18th frequency variations are ±12.0 Hz, ±24.0 Hz and ±36.0 Hz, respectively. The Bode diagram of $G_{ui}(s)$ with feed-forward regulator is plotted as Fig.7 when the grid fundamental frequency is equal to 48Hz.

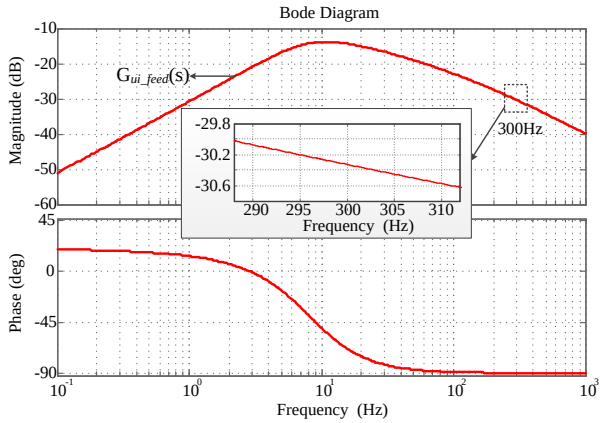

Fig.11 Bode diagram of $G_{ui}(s)$ with feed-forward regulator when fundamental frequency with 2Hz deviation

As can be seen from Fig.10, the magnitude response is almost -30dB at 288Hz (6th harmonic frequency), -34.6dB at 576Hz (12th harmonic frequency), -39.4dB (18th harmonic frequency) which still has a good attenuation ability against the grid harmonic voltages. Thus, the feed-forward regulator has good robustness against grid frequency variations.

D. *Robustness against DFIG parameter deviations*

As can be seen from (14), the ideal feed-forward regulator is depended on the ratio of rotor inductance and mutual inductance, which is simplified as one in the actual feed-forward regulator. However, the DFIG parameters may change due to the temperature, the skin effects and the flux linkage saturation, etc [19]. Consequently, it is essential to discuss the robustness of the proposed control strategy against the parameter deviations.

The control performance of the actual feed-forward regulator depends on the ratio of the rotor inductance and mutual inductance. The error between the ideal and actual feed-forward regulator can be expressed as,

$$\frac{L_r}{L_m}-1=\frac{L_{\delta r}}{L_m} \tag{22}$$

As can be seen from (21), the error is always greater than zero and monotonous. Thus, if the attenuation magnitude of the $G_{\mathrm{ui}}(s)$ can be achieved even when the biggest error occurs, the feed-forward regulator will be practically useful during the DFIG parameter variations. The variation range of rotor leakage inductance and the mutual inductance is usually ± 20% [18]. When the rotor leakage inductance increases 20% and the mutual inductance decrease 20%, the error is biggest.

itation information: DOI 10.1109/TPEL.2017.2677527, IEEE

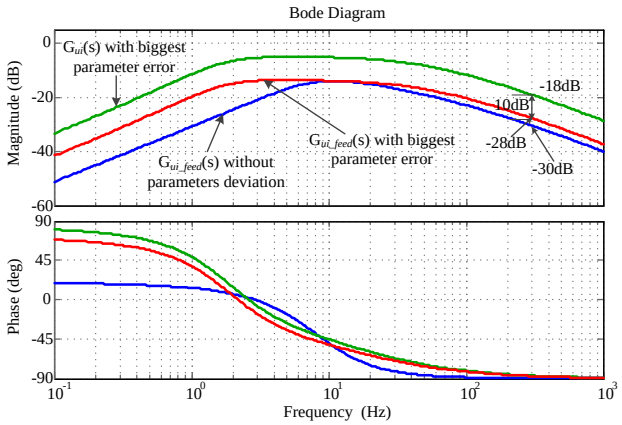

Fig.12 Bode diagram of G_{ui}(s) with biggest parameter deviation

As can be seen from Fig.9, the attenuation amplitude decreases to 10dB compared with Fig.8 which is introduced by the parameters error. However, the magnitude response of the G_{ui}(s) without feed-forward regulator will decrease to -18dB when the rotor leakage inductance increases 20% and the mutual inductance decrease 20%. And the magnitude response of the G_{ui}(s) with feed-forward regulator can still be -28dB in the biggest parameter variation condition. Thus, the stator harmonic currents suppression ability can still be ensured in this condition. The feed-forward regulator has good robustness against DFIG parameter deviations.

E. Phase compensation of the harmonics

When the system delay is considered, the linear phase compensation of the harmonics is necessary for the control accuracy. The system delay is always considered as 1.5 sampling period.

In this paper, a leading phase compensator is added in the control scheme when the sampling frequency is low. The phase delay of each harmonics can be expressed as,

$$\theta_n = 1.5T_s\omega_n \tag{23}$$

Where ω_n is the nth order harmonic frequency, T_s is the sampling period, θ_n is the phase delay of the nth order harmonic frequency.

The ideal leading phase compensator can be expressed as,

$$G_{ideal\_lead}(s) = e^{1.5T_s s} \tag{24}$$

However, this ideal leading phase compensator cannot be used in the practical application since it is a non-causal block. In order to compensate the phase delay of the high order harmonics, a practical leading phase compensator is designed as,

$$G_{lead}(s) = k_{lead}\frac{s+\omega_b}{s+\omega_a} \tag{25}$$

The phase of the leading phase compensator can be expressed as,

$$\theta_{lead} = \arctan\left(\frac{\omega}{\omega_b}\right) - \arctan\left(\frac{\omega}{\omega_a}\right) \tag{26}$$

As can be seen from (24), the phase delay of each harmonics is a linear phase delay. Thus, the phase of the leading phase compensator also needs to be designed linearly with the frequency. However, the leading phase in (26) is nonlinear with the frequency. As known, the harmonic frequency in the grid voltage varies from 100Hz to 1000Hz, in this way, the leading phase can be designed linearly in this range. If ω_a and ω_b are much larger than ω, (26) can be approximated as,

$$\theta_{lead} \approx \frac{\omega}{\omega_b} - \frac{\omega}{\omega_a} = \frac{\omega_b - \omega_a}{\omega_a\omega_b}\omega \tag{27}$$

Furthermore, if ω_2 are much larger than ω_1, this expression can be rewritten as,

$$\theta_{lead} \approx \frac{1}{\omega_b}\omega \tag{28}$$

In this way, the ω_b can be gotten by

$$\omega_b = \frac{1}{1.5T_s} \tag{29}$$

When T_s is equal to 0.1ms which means that the sampling frequency is 10KHz, ω_b is 6667, ω_a should be much greater than ω_b and is designed as 100000*pi, and k_{lead} is almost equal to ω_a/ω_b which can guarantee the unity gain and the stator fundamental voltage is not effected .

The bode diagram of the practical leading phase compensator and ideal phase compensator can be shown as Fig.13.

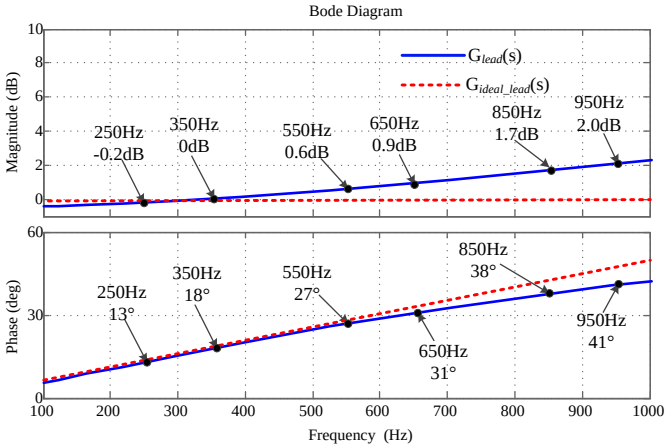

Fig.13 The bode diagram of the ideal and practical leading phase compensator

TABLE I The harmonic phase of phase compensator

	250Hz	350Hz	550Hz	650Hz	850Hz	950Hz
Ideal phase compensator	13.5°	18.9°	29.7°	35.1°	45.9°	51.3°
Actual phase compensator	13°	18°	27°	31°	38°	41°

As can be seen from the Fig.13 and table I , the phase error between the practical phase compensator and the ideal phase compensator are less than 5° when the frequency is less than 650Hz, which is acceptable in the practical application. When the harmonic frequency is higher, the phase error increases because the error of arc tangent linearization increases. Thus, the ability of suppressing the high order harmonics at 850Hz and 950Hz will be deteriorated. However, these harmonic components at the grid voltage are relatively small and has little impact on the THD of the stator harmonic current. The 5th, 7th ,11th and 13th stator harmonic currents can be effectively eliminated even at low sampling frequency. Thus, the feed forward regulator is still effective in suppressing the stator harmonic currents even the sampling frequency is low with the leading phase compensator.

itation information: DOI 10.1109/TPEL.2017.2677527, IEEE

V. Simulation Results

The performance of the proposed control method is first verified by simulations in MATLAB/Simulink and then realized and tested in the laboratory. The parameters of DFIG applied in the simulation are shown as Table I which are the same as the experimental system. The simulation results are divided into two parts, namely the comparison between the resonant controller and the feed forward regulator, the performance of the proposed control method during grid voltage sag. The control scheme is implemented in a per unit system.

A. Comparing with Resonant controller

In order to compare the dynamic performance of the feed forward regulator and the resonant controller, the simulation of DFIG with the resonant controller and with the feed forward regulator are conducted. In the simulation, the distorted grid voltage only contains the 5th- and the 7th- order harmonic components which are both set as 7.14%. The rotor speed is initially set to 800r/min, while the synchronous speed is 1000r/min.

Fig.14(a) shows the simulation results of DFIG under distorted grid voltage without and with the resonant controller. The active power is set as 0.5pu and the reactive power is set as 0pu. During the period 0-0.1s, the resonant controller is not enabled. The 5th order harmonic and 7th order harmonic component in the stator current are 4.81% and 3.71% respectively. At 0.1s, the resonant controller is enabled and the steady state operation can be obtained within 21ms. In the steady state with the resonant controller, the 5th order harmonic and 7th order harmonic component in the stator current are 0.23% and 0.16% respectively.

Fig.14(b) shows the simulation results of DFIG under distorted grid voltage without and with the feed forward regulator. The working condition is the same as Fig.14(a). During the period 0-0.1s, the feed forward regulator is not enabled. At 0.1s, the feed forward regulator is enabled and the steady state operation can be obtained within 2ms. In the steady state with the feed forward regulator, the 5th order harmonic and 7th order harmonic component in the stator current are 0.76% and 0.58% respectively.

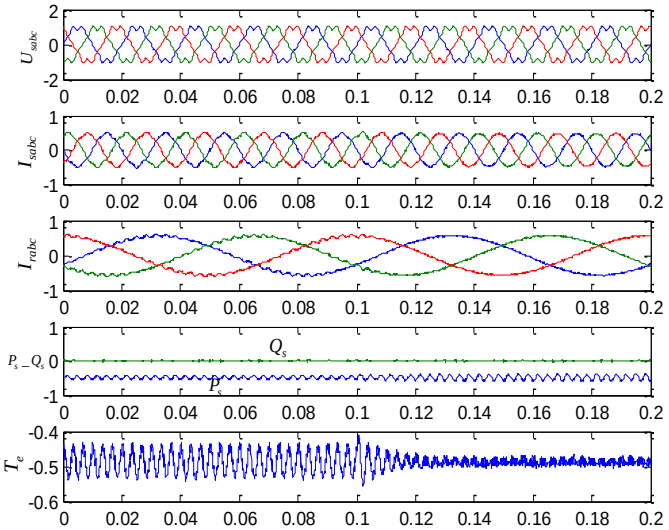

(a)

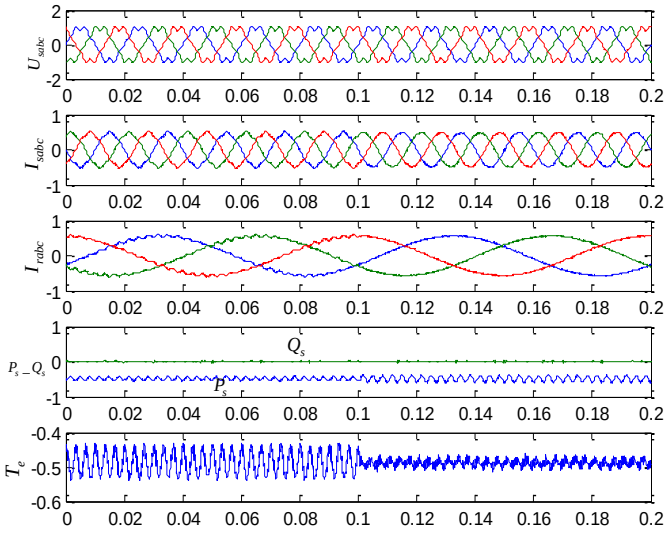

(b)

Fig.14 Simulation results of DFIG under distorted grid voltage (a) with resonant controller (b) with feed forward regulator

Comparing Fig.14(a) with Fig.14(b), the steady performance of the resonant controller is better than the feed forward regulator because the magnitude response of G_{ui}(s) with feed forward regulator is -30dB and the magnitude response is -39dB with the resonant controller. Both of these two methods are effective in suppressing the stator harmonic currents. However, the dynamic performance of the feed forward regulator is better than the resonant controller which conforms to the theoretical analysis.

B. During the grid voltage sag

In order to validate that the dynamic performance of the stator fundamental current is not decreased by the feed forward regulator. The simulation results of DFIG under the grid voltage sag with and without the feed forward regulator are conducted. There is no harmonic considered in this simulation condition.

Fig.15(a) shows the simulation results of the DFIG under a sudden grid voltage dip to the 50% of rated grid voltage without the feed forward regulator. The active and reactive current reference is kept as 1pu and 0pu respectively. At 0.1s, the stator voltage dips to 0.5pu suddenly. From 0.1s to 0.4s, the power and the torque is oscillated due to the static stator flux linkage components, and these pulsations are attenuated in 350ms.

Fig.15(b) shows the simulation results of the DFIG under a sudden grid voltage dip to the 50% of rated grid voltage with the feed forward regulator. The active and reactive current reference is also kept as 1pu and 0pu respectively. At 0.1s, the stator voltage reduces to 0.5pu suddenly. From 0.1s to 0.4s, the power and the torque is oscillated due to the static stator flux linkage components, and these pulsations are attenuated in 350ms.

Thus, the dynamic performance of the DFIG under sudden voltage sag without and with the feed forward regulator are almost the same which can be seen from Fig.15(a) and Fig.15(b), which also validates that the dynamic performance of the stator fundamental current is not decreased by the feed forward regulator.

itation information: DOI 10.1109/TPEL.2017.2677527, IEEE

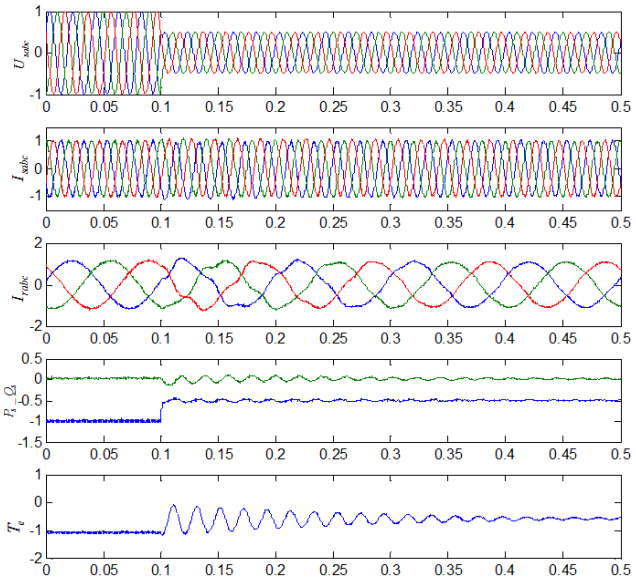

(a)

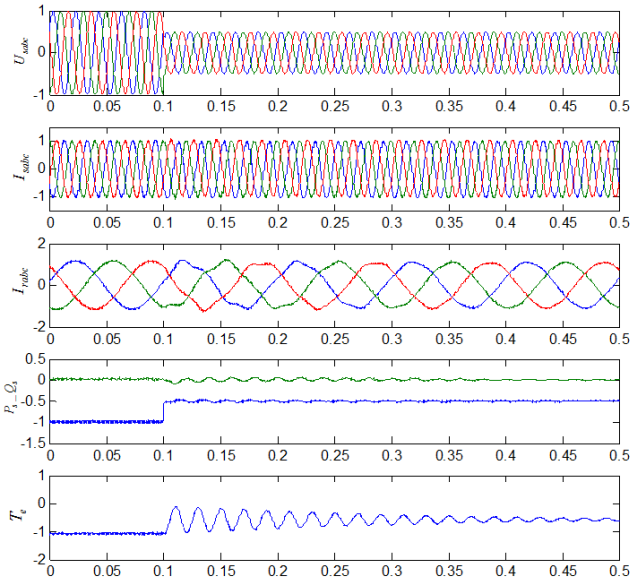

(b)

Fig.15 The simulation results of DFIG during voltage sag (a) without feed forward regulator (b) with the feed forward regulator

VI. Experimental Results

In order to validate the control strategy proposed in section III, a DFIG-based experimental system is developed. The schematic diagram of the experimental system is shown in Fig. 16. The DFIG was driven by a squirrel cage induction motor with the control of general inverter. The Chroma 61704 programmable three-phase voltage source is set up to emulate the harmonic distorted power grid. The control strategy of RSC is implemented on the TI TMS320F28335 DSP and the switching frequency is 10 kHz with a sampling frequency of 10 kHz. The parameters of the DFIG are shown in Table II. All the waveforms are acquired by a YOKOGAWA DL750 scope.

In the experiment, firstly the distorted grid voltage only contains the 5th- and the 7th- order harmonic components which are set as 6.09% and 3.91% respectively. The rotor speed is initially set to 800r/min, while the synchronous speed is 1000r/min.

TABLE II Parameters of the tested DFIG

Rated power	1.0kW	Rated voltage	110V
Rated frequency	50Hz	DC voltage	300V
Stator/Rotor turns ratio	0.33	L_m	87.5mH
R_s	1.01Ω	R_r	0.88Ω
$L_{\delta s}$	5.6mH	$L_{\delta r}$	5.6mH

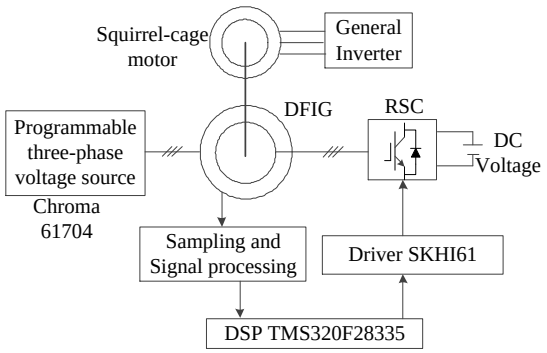

Fig.16 The schematic diagram of the experimental system

Fig.17 shows the steady state experimental results of DFIG system when the feed-forward regulator is disabled. In the experimental tests, the active power reference of the stator is -500W and reactive power reference of the stator is 0Var. The minus sign represents that the energy flows from the DFIG stator to the grids. The rotor speed is 800rpm and the fundamental frequency of the stator is 50Hz. In the experimental results, the harmonics of the stator current are mainly at 250Hz and 350Hz, which are 10.38% and 5.21% respectively, which is harmful for the output power quality. These harmonics in the stator current will also lead to the ripple which are mainly at 300Hz in the stator power and torque. The torque ripple is ±0.23N.m (4.89%) and the ripple of the active power and reactive power are ±31W(6.21%) and ±26.6Var(5.32%), respectively.

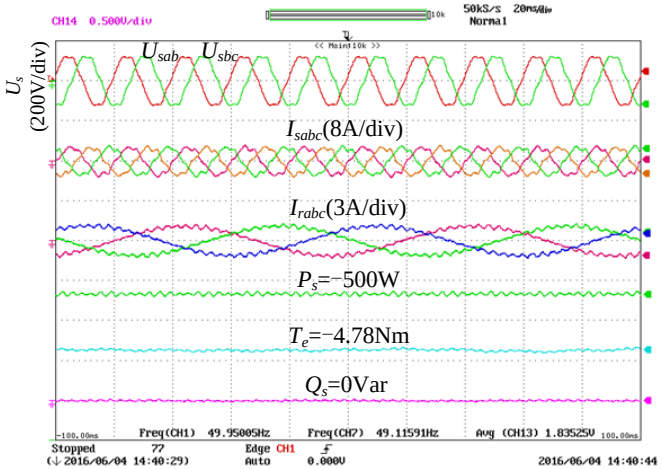

Fig.17 Experimental results of DFIG under distorted grid voltage without enabling the feed-forward regulator

Fig.18 shows the steady state experimental results of DFIG system when the feed-forward regulator is enabled. The active power reference and reactive power reference are the same with Fig.17. As can be seen from the figure, the harmonics of the stator and rotor currents are mitigated simultaneously, which

itation information: DOI 10.1109/TPEL.2017.2677527, IEEE

corresponds with the theoretical analysis. The harmonics of the stator current are mainly at 250Hz and 350Hz, which have been reduced to 2.62% and 2.25%, respectively. Thus, the feed-forward regulator works well in suppressing the stator harmonic currents. And the torque ripple also decreases to 1.12% and the ripple of the active power and reactive power are 4.18% and 2.79%, respectively.

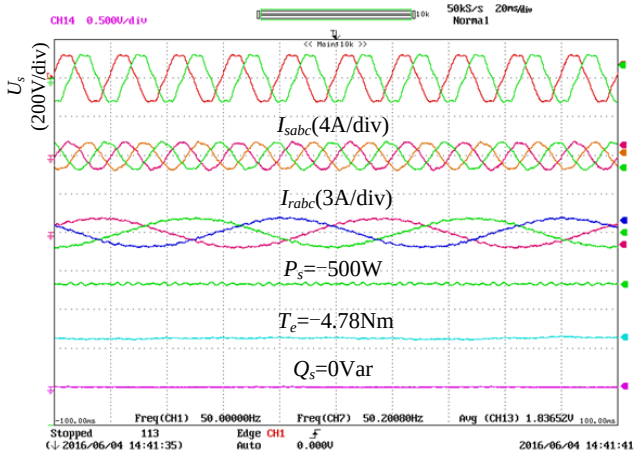

Fig.18 Experimental results of DFIG under distorted grid voltage with enabling the feed-forward regulator

Fig.19 is the experimental results with the step response from -200W to -600W of the stator active power reference when the feed-forward regulator is enabled. It can be seen that the active power of DFIG rises to the reference in less than 30ms without any overshoot. The amplitude of the stator phase current changes from 1.48A to 4.45A and the amplitude of the rotor phase current changes from 0.9A to 1.67A. The electromagnetic torque increases from 1.91Nm to 5.73Nm. As can be seen from the figure, the DFIG system has good dynamic and steady response under distorted grid voltage with the feed-forward regulator enabled when the stator active power reference changes suddenly.

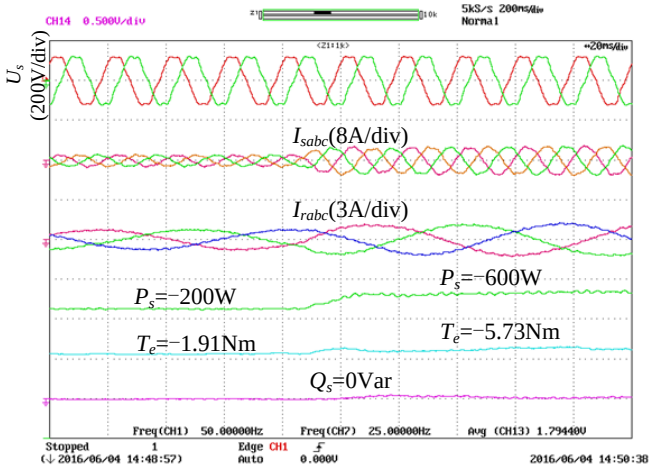

Fig.19 Experimental results of DFIG output active power stepping under distorted grid voltage with enabling the feed-forward regulator

Fig.20 is the experimental result of DFIG when the rotor speed changes from 900r/min to 1100r/min. The stator active power reference is set to -500W and the feed-forward regulator is enabled. The harmonics in the stator current are the same with Fig.18 which is operating at the constant rotor speed. Furthermore, the stator power and the electromagnetic torque are stable during the rotor speed variation. Thus, the DFIG system also has good dynamic response under distorted grid voltage with the feed-forward regulator enabled when DFIG operates on the sub-synchronous and super-synchronous speed.

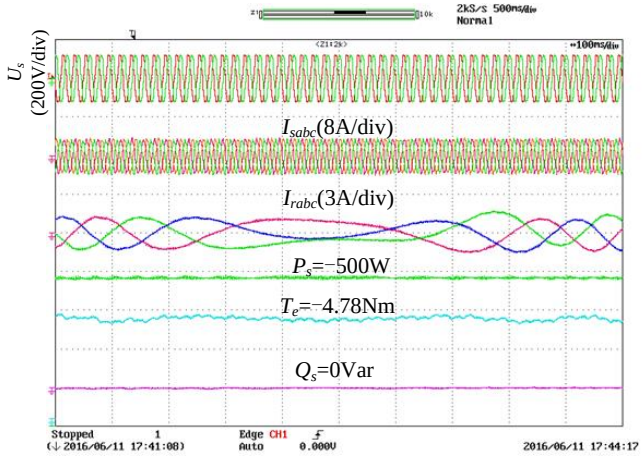

Fig.20 Experimental results of DFIG during rotor speed variation under distorted grid voltage with enabling the feed-forward regulator

In order to investigate the robustness of the DFIG system against grid frequency variation with the feed-forward regulator, the condition in which the fundamental frequency of the grid changes from 50Hz to 48Hz suddenly is conducted in Fig.21. The harmonics in the grid voltage are the same with Fig.18. As can be seen from the figure, the harmonics in the stator current can still be reduced even the grid frequency changes to 48Hz and the overshoot of the stator current is small in the dynamic process. When the fundamental frequency changes 2Hz, the sixth order harmonic in the *dq* frame changes 12Hz, which is almost 75rad/s deviation of the resonant frequency. It is difficult to use the bandwidth of the resonant regulator to control the harmonic current at the resonant frequency, while the feed-forward regulator is still suitable in the frequency variation situation.

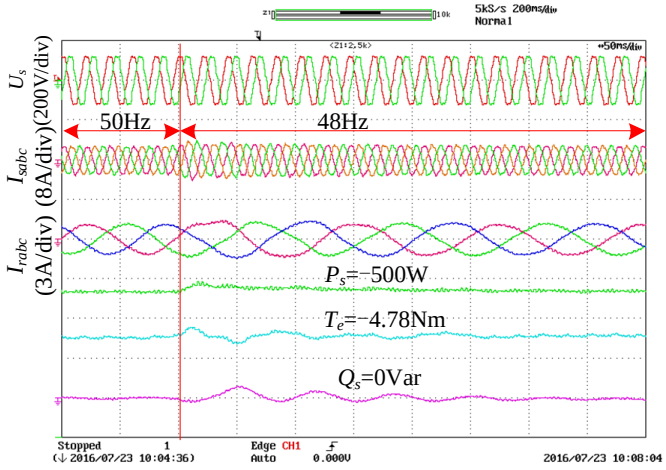

Fig.21 Experimental results of DFIG under distorted grid voltage with enabling the feed-forward regulator when the grid fundamental frequency changes from 50Hz to 48Hz

 itation information: DOI 10.1109/TPEL.2017.2677527, IEEE

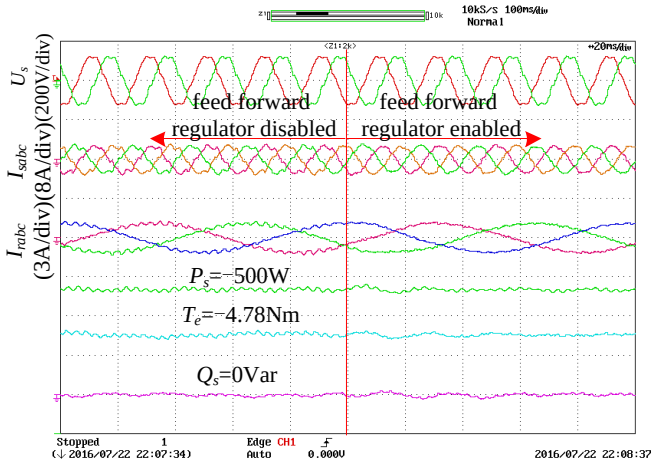

Fig.22 Experimental results of DFIG under generalized harmonic grid voltage

Fig. 22 shows the experimental results of DFIG under the generalized harmonic grid voltage, in which 5th, 7th, 11th, 13th, 17th, and 19th order harmonic components of the grid voltage are set as 5.98%, 3.83%, 2.76%, 2.12%, 1.87%, and 1.67%, respectively. When the feed-forward regulator is disabled, the stator harmonic currents at 5th, 7th, 11th, 13th, 17th, and 19th order are 10.12%, 5.25%, 2.47%, 1.87%, 1.76% and 1.37% respectively. When the feed-forward regulator is enabled, the stator harmonic currents at 5th, 7th, 11th, 13th, 17th, and 19th order are reduced to 2.65%, 2.01%, 1.47%, 1.17%, 0.97% and 0.74% respectively. Thus, it can be proved that the proposed feed-forward regulator is capable to work well in suppressing the stator harmonic currents even under the generalized harmonic grid.

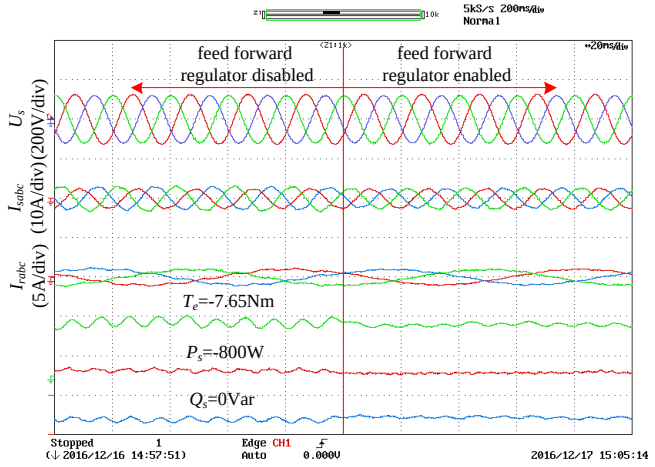

Fig.23 experiment results of DFIG under unbalanced grid voltage with and without the feed forward regulator

In the experiment of unbalanced grid voltage conditions, the voltage unbalanced factor (VUF) is set as 5%. The stator active power reference is -800W and the stator reactive power is 0 Var. The experiment results under the unbalanced grid voltage with the feed forward regulator disabled and enabled are shown in Fig. 23. As can be seen from this figure, the stator current unbalanced factor is 8.56% when the feed forward regulator is disabled. Then when the feed forward regulator is enabled, the stator current unbalanced factor is 0.89%. Furthermore, the ripples of the stator power and the electromagnetic torque are decreased by applying the feed forward regulator since the stator negative sequence currents are suppressed effectively. Therefore, the feed forward regulator is also effective in suppressing the stator negative sequence currents under the unbalanced grid voltage.

VII. Conclusions

The contribution of the paper is to suppress the stator harmonic currents of DFIG using the feed-forward regulators under generalized distorted grid voltage. The conclusion can be highlighted as follows.

1. The direct stator current control is applied for the stator fundamental current control without using rotor current vector control. The parameter dependency can be reduced when calculating the current reference.
2. The feed-forward regulator is employed for stator harmonic currents control, which has good robustness against grid frequency variations and DFIG parameter deviations.
3. In the proposed control strategy for the suppression of the stator harmonic current, the resonant controller is removed and the design of the gain and bandwidth of the resonant controller can be avoided.

As can be seen from the experimental result, the proposed feed-forward regulator has good dynamic and steady response during the stator power variation, rotor speed changing and grid frequency deviation.

References

[1] R. Cardenas, R. Pena, S. Alepuz, and G. Asher, “Overview of control systems for the operation of DFIGs in wind energy applications,” *IEEE Trans. Ind. Electron.*, vol. 60, no. 7, pp. 2776-2798, Jul, 2013.

[2] F. Blaabjerg, M. Liserre and K. Ma, “Power electronics converters for wind turbine systems,” *IEEE Trans. Ind. Appl.*, vol.48, no.2, pp. 708-719, Mar-Apr. 2012.

[3] M. Tazil, V. Kumar, R. C. Bansal, S. Kong, Z. Y. Dong and W. Freitas, “Three-phase doubly fed induction generators: An overview”, *IET Electr. Power Appl.*, vol.4, no.2, pp. 75-89, Aug. 2010.

[4] L. Fan and S. Yuvarajan, “Harmonic analysis of a DFIG for a wind energy conversion system,” *IEEE Trans. Energy Convers.*, vol. 25, no. 1, pp. 181-190, March 2010.

[5] H. Nian and Y. Song, “Direct power control of doubly fed induction generator under distorted grid voltage,” *IEEE Trans. Power Electron.*, vol. 29, no. 2, pp. 894–905, Feb. 2014.

[6] J. Hu, H. Nian, H. Xu, and Y. He, “Dynamic Modeling and Improved Control of DFIG under Distorted Grid Voltage Conditions,” *IEEE Trans. Energy Convers.*, vol. 26, no. 1, pp. 163-175, March 2011.

[7] H. Xu, J. Hu, and Y. He, “Operation of Wind-Turbine-Driven DFIG Systems Under Distorted Grid Voltage Conditions: Analysis and Experimental Validations,” *IEEE Trans. Power Electron.*, vol. 27, no. 5, pp. 2354-2366, May 2012.

[8] H. Xu, J. Hu, Y. He, “Integrated Modeling and Enhanced Control of DFIG Under Unbalanced and Distorted Grid Voltage Conditions,” *IEEE Trans. Energy Convers.*, vol. 27, no.3, Sep 2012.

[9] V.T. Phan, H. H. Lee, “Control strategy for harmonic elimination in stand-alone DFIG applications with nonlinear loads,” *IEEE Trans. Power Electron.*, vol.26, no.9, pp.2662-2675, Sep.2011.

[10] V.T. Phan, H.H. Lee, “Performance enhancement of stand-alone DFIG systems with control of rotor and load side converters using resonant controllers”, *IEEE Trans. Ind. Electron.*, vol.48, no.1, pp.199-210, Jan.2012.

[11] A. G. Yepes, F. D. Freijedo, J. Doval-Gandoy, O. Lopez, J. Malvar, and P. Fernandez-Comesana, “Effects of discretization methods on the performance of resonant controllers,” *IEEE Trans. Power Electron.*, vol. 25, no. 7, pp. 1692–1712, Jul. 2010.

 itation information: DOI 10.1109/TPEL.2017.2677527, IEEE

[12] C. Liu, F. Blaabjerg, W. Chen, and D. Xu, "Stator current harmonic control with resonant controller for doubly fed induction generator," *IEEE Trans. Power Electron*., vol. 27, no. 7, pp. 3207–3220, Jul. 2012.

[13] X. Wang, F. Blaabjerg, and Z. Chen, "Autonomous control of inverter - interfaced distributed generation units for harmonic current filtering and resonance damping in an islanded microgrid," *IEEE Trans. Ind. Appl.*, vol. 50, no. 1, pp. 452-461, Jan.-Feb. 2014.

[14] Y. Song and H. Nian, "Sinusoidal output current implementation of DFIG using repetitive control under a generalized harmonic power grid with frequency deviation," *IEEE Trans. Power Electron.*, vol. 30, no. 12, pp. 6751–6762, Dec. 2015.

[15] Yipeng Song, Heng Nian, "Enhanced grid-Connected operation of DFIG using improved repetitive control under generalized harmonic power grid," *IEEE Trans. Energy Convers.*, vol. 30, no.3, Sep 2015.

[16] Yipeng Song, Heng Nian, "Modularized control strategy and performance analysis of DFIG system under unbalanced and harmonic Grid Voltage," *IEEE Trans. Power Electron.*, vol. 30, no. 9, pp. 4831–4842, Sep. 2015.

[17] F. Wei, X. Zhang, D. M. Vilathgamuwa, S. S. Choi, and S. Wang, "Mitigation of distorted and unbalanced stator voltage of stand-alone doubly fed induction generators using repetitive control technique," *IET Electron Power Appl.*, vol. 7, no. 8, pp. 654–663, 2013.

[18] P. Xiong, D. Sun, "Backstepping-based DPC strategy of a wind turbine-driven DFIG under normal and harmonic grid voltage," *IEEE Trans. Power Electron.*, vol. 31, no. 6, pp. 4216–4225, Jun. 2016.

[19] P. Cheng, H. Nian, Chao Wu and Z. Zhu, "Direct stator current vector control strategy of DFIG without phase locked loop during network unbalance," *IEEE Trans. Power Electron.*, vol. 32, no. 1, pp. 284–297, Jan. 2017.

[20] H. Nian, Y. Song, "Optimised parameter design of proportional integral and resonant current regulator for doubly fed induction generator during grid voltage distortion," *IET Renew. Power Gener.*, vol.8, no.3, pp.299-313, Jun, 2014.

[21] E. Kurniawan, Z. Cao, and Z. Man, "Design of robust repetitive control with time-varying sampling periods," *IEEE Trans. Ind. Electron.*, vol. 61, no. 6, pp. 2834–2841, Jun. 2014.

[22] V.T. Phan, D.T. Nguyen, "Harmonics rejection in stand-slone doubly-fed induction generators with nonlinear loads," *IEEE Trans. Energy Convers.*, vol. 31, no.2, Sep 2016.

[23] N.K. Swami, Bhim Singh, "Doubly fed Induction generator for wind energy conversion systems with integrated active filter capabilities", *IEEE Trans. Ind. Informatics.*, vol. 61, no. 6, pp. 2834–2841, Jun. 2014.

[24] Saeed Golestan, Josep M. Guerrero, Juan C. Vasquez, "Three-phase PLLs: A review of recent advances," *IEEE Trans. Power Electron.*, vol. 32, no. 3, pp. 1894–1907, Mar. 2017.

[25] Y. Yang, K. Zhou, M. Cheng, etc "Phase Compensation Multiresonant Control of CVCF PWM Converters," *IEEE Trans. Power Electron.*, vol. 28, no. 8, pp. 3923–3930, Aug. 2013.

Chao Wu was born in Huanggang, China, in 1992. He received the B.Eng. degree in electrical engineering from HeFei University of Technology, Hefei, China. He is currently working toward the Ph.D. degree in electrical engineering in Zhejiang University, Hangzhou, China.

His current research interests are mainly on the control strategy of doubly fed induction generators for DC power transmission in wind energy conversion systems.

Heng Nian (M'09，SM'14) received the B.Eng. degree and the M.Eng. degree from HeFei University of Technology, China, and the Ph.D. degree from Zhejiang University, China, in 1999, 2002, and 2005 respectively, all in electrical engineering. From 2005 to 2007, he was as a Post-Doctoral with the College of Electrical Engineering, Zhejiang University, China.

Since 2007, he has been employed as an associate professor at the College of Electrical Engineering, Zhejiang University, China. His current research interests include the optimal design and operation control for wind power generation system.